Supplemental Information

Behavior Reveals Selective

Summation and Max Pooling

among Olfactory Processing Channels
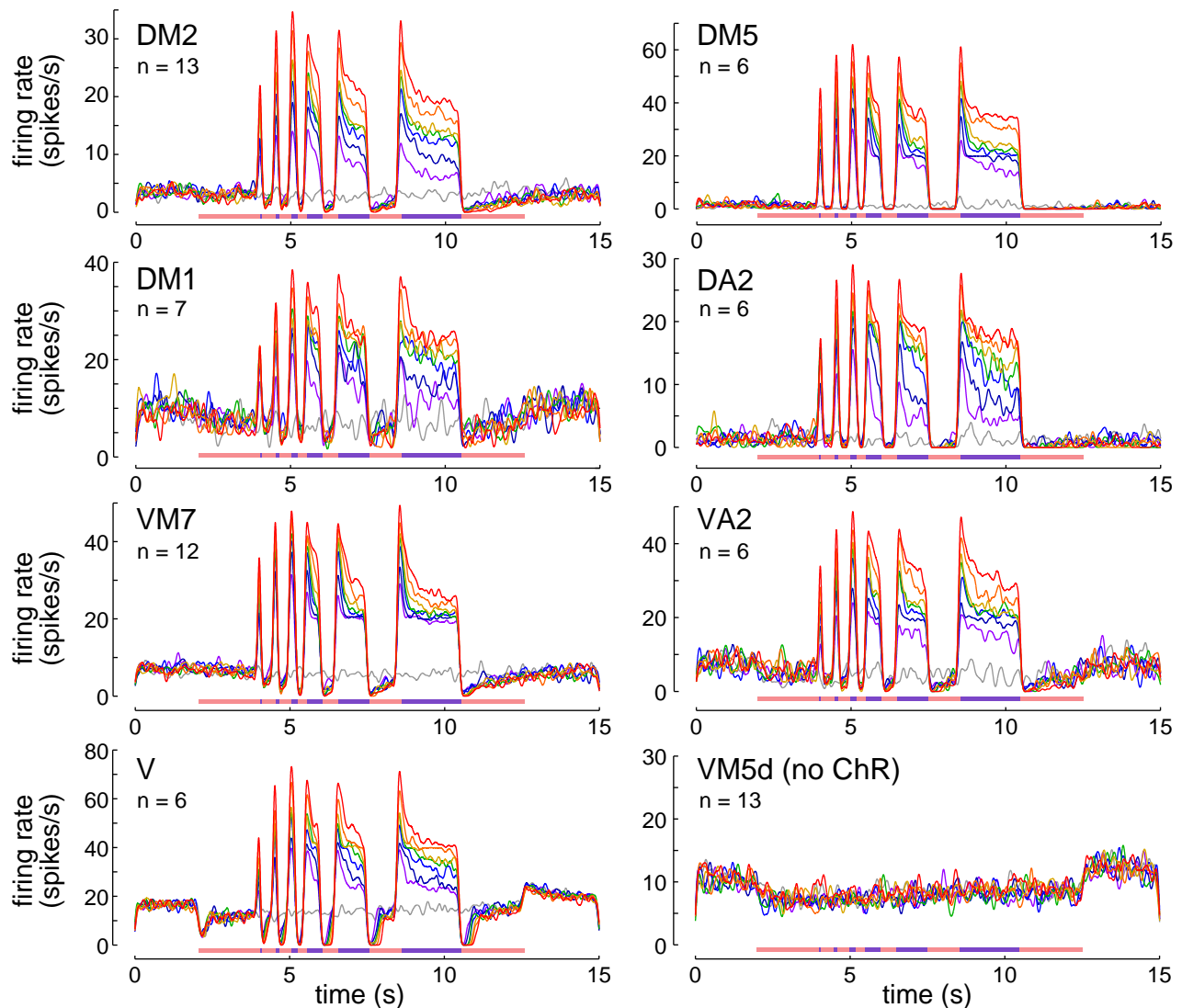
Joseph S. Bell and Rachel I. Wilson

Figure S1: Light evokes steadily increasing firing rates in channelrhodopsin-expressing ORNs.

Firing rates were measured from seven ChR-expressing ORN types, plus one control ORN type that did not express ChR (VM5d). Each plot shows mean ORN firing rate versus time (averaged over all recordings from that ORN type). Warmer colors indicate increasing blue light intensity (gray = 0 mW/mm^2, red = 1.5 mW/mm^2). Note that firing rates continue to increase as blue light intensity grows, even toward the maximum end of the light intensity series. Note also that the intensity-dependence and temporal pattern of these firing rates were relatively similar across ORN types. DM2 data are reproduced from **Figure 1B**.

Every trial began with 2 s of baseline recording, after which we began an alternating sequence of blue and red light presentations, meant to mimic the stimuli a fly might experience in the behavior chamber. In trials where blue light power was maximum, the blue flashes consisted of 1.5 mW/mm^2 blue light. In trials where blue light power was less than maximum, the "blue" flashes consisted of a mixture of red and blue light, where total light intensity (red + blue) was always 1.5 mW/mm^2. The red flashes were always 1.5 mW/mm^2, meaning total intensity was always held constant at a fixed value during every 10-s stimulus epoch. This thermal compensation procedure was the same as that used in the behavioral experiments (see Supplemental Experimental Procedures).

Red light produced a slight suppression of baseline firing rate in ORNs, including the ORNs that did not express ChR. In the ORNs presynaptic to glomerulus V, this suppression was larger than in other ORN types.
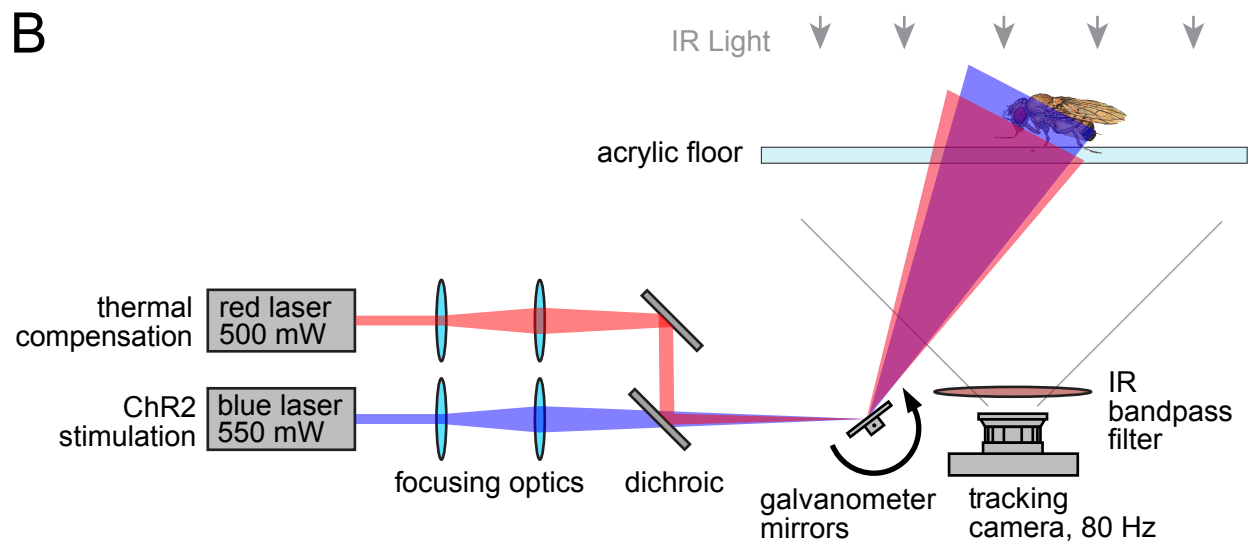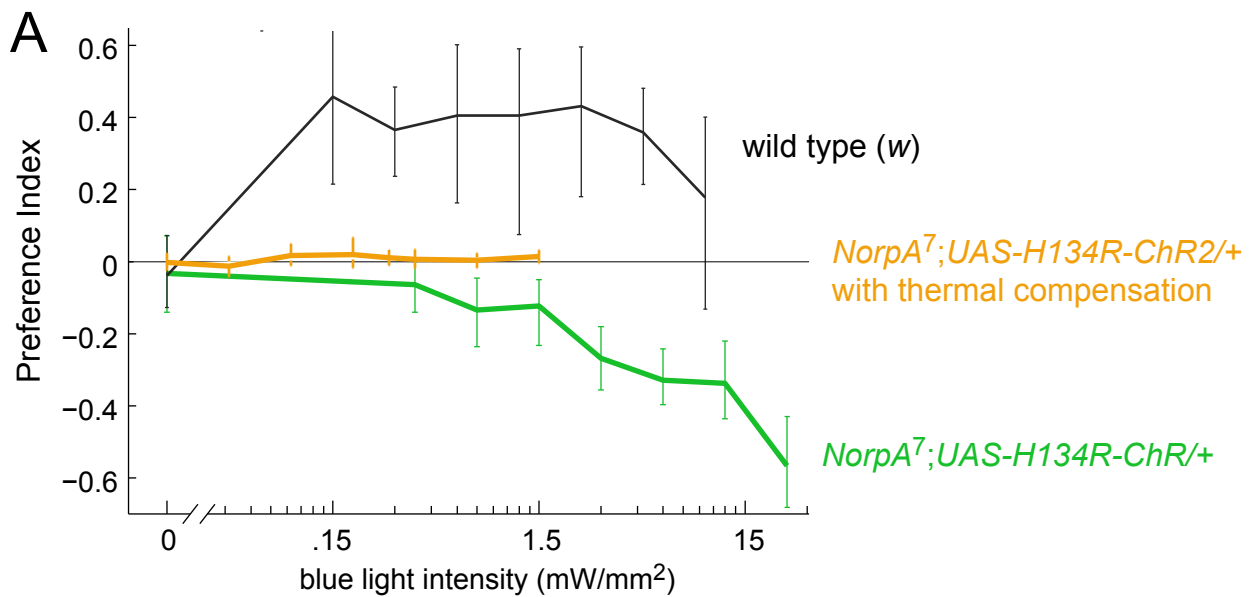
Figure S2: Thermal compensation with the red laser effectively eliminates biases in the Preference Index in blind flies.

(A) Mean Preference Index versus blue light intensity (± bootstrapped 95% confidence intervals). Wild type flies walk toward the blue laser (w background, n = 8 flies), whereas $NorpA^7$ mutants avoid the blue laser at high intensities (n = 16 flies), presumably because the blue half of the chamber is warmer (there is no red laser in these trials). With red-laser thermal compensation, $NorpA^7$ mutants show no preference for the blue versus red halves of the chamber (n = 64 flies). In these latter experiments, both the red and blue light was 1.5 mW/mm^2.

(B) Schematic of the optical path to fly. Red and blue diode lasers are combined with a dichroic mirror, and then steered to the fly via a 2-axis scanning galvanometer mirror system driven by real-time video tracking. Each fly receives pulses from the red and blue laser at 20 Hz (see Supplemental Experimental Procedures).
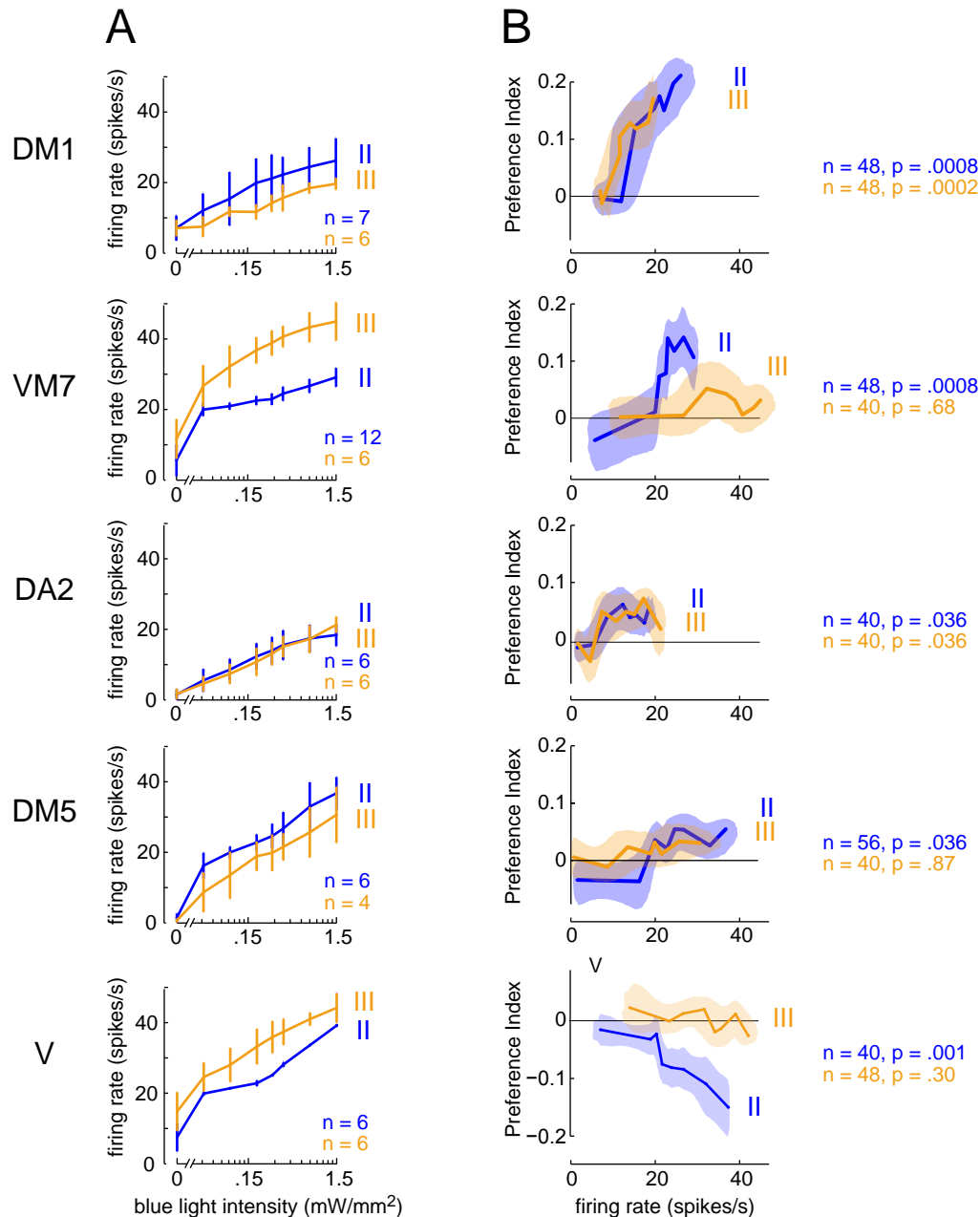
Figure S3: Different Gal4 lines driving expression in the same ORNs can elicit different ORN firing rates and different levels of behavior.

(A) ORN firing rates versus blue light intensity (± s.d. across ORNs) for the five ORN types where we were able to compare the effects of two alternative Gal4 lines. The Gal4 lines used in **Figure 4** are shown in blue, with alternative genotypes (not in **Figure 4**) shown in gold. Roman numeral indicate the chromosome that the transgene was inserted on. Details of each Gal4 line are listed in **Table S2**. In some cases, the two alternative Gal4 lines drive different ORN firing rates, potentially due to differences in the level of channelrhodopsin expression. In two cases (VM7 and V), there are also differences between the two genotypes in baseline (zero-blue-laser) firing rates

.
(B) PI versus ORN firing rate for the same pairs of Gal4 lines. Shaded bands show bootstrapped 95% bivariate confidence intervals, calculated as in **Figure 4** (see Supplemental Experimental Procedures). P-values represent comparisons with control flies that do not express ChR ("No Gal4" control; see Supplemental Experimental Procedures). For three of these glomeruli, the two Gal4 lines drive similar levels of behavior; for these two glomeruli there is also reasonable congruence between the two ORN firing rate curves. For two glomeruli (VM7 and V), there is a substantial difference in the level of behavior elicited by a given blue light intensity. In both these cases, the Gal4 line with higher light-evoked firing rates (and also higher baseline firing rates) actually elicits weaker behavior. This implies that the ORN-behavior curve is in fact different in the two Gal4 lines, indicating a difference in the way that the central nervous system responds to ORN spikes. Thus, it is likely that the differences between the two Gal4 lines are attributable to different levels of central adaptation. The idea that there is central adaptation is also consistent with our finding that we could increase the level of behavior by scaling down the entire series of blue light intensities that we used over the course of a day's experimental run (**Figure S4**).
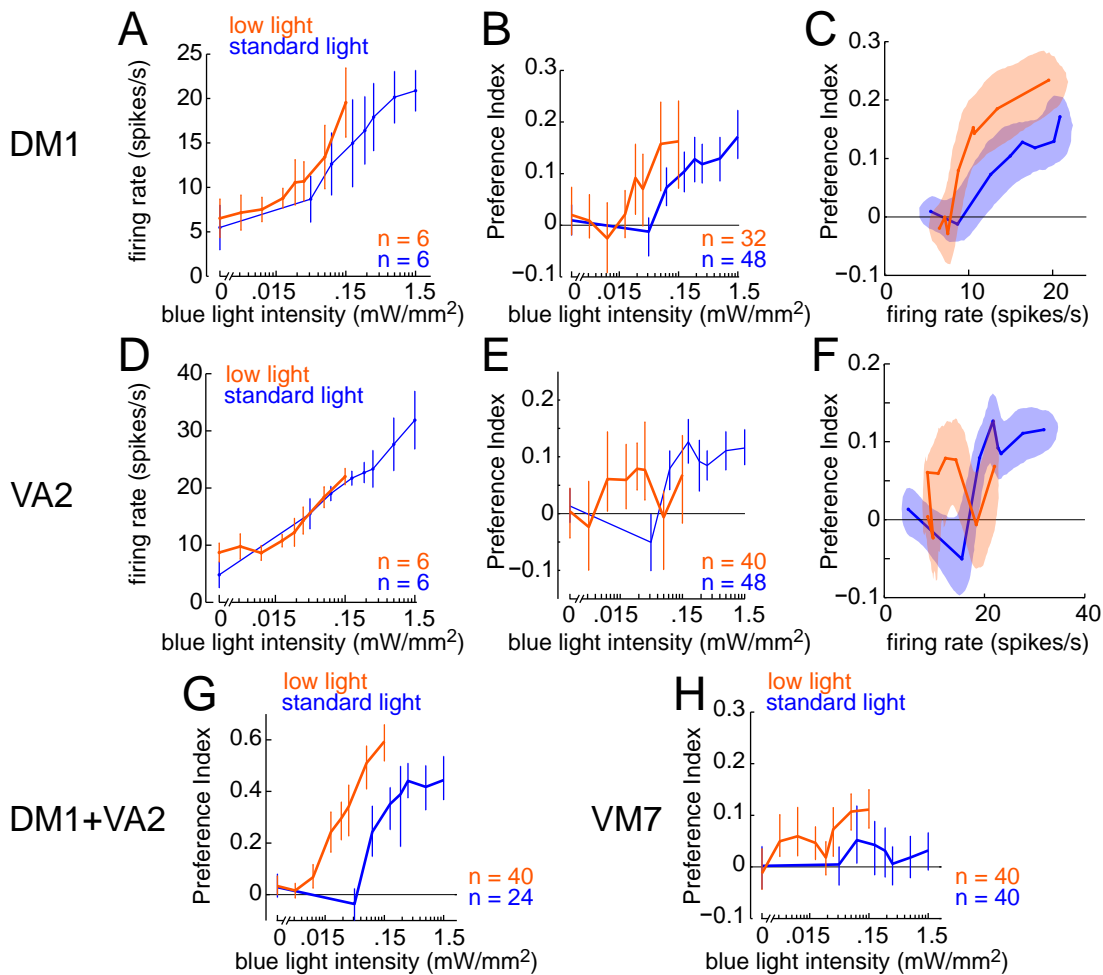
Figure S4: Higher overall blue light intensities produce adaptation in behavior.

In all the experiments in the main figures and analyses of this study, we used a graded series of blue light intensities with a maximum intensity of 1.5 mW/mm^2. Here we tested the effect of scaling down the entire series of blue light intensities 10-fold, so that the average amount of blue light delivered over the course of the experiment would be 10-fold lower. Each experiment lasts 8 hours, and different light intensities are interleaved, so if there is any long-timescale adaptation elicited by high light levels, we might expect to see that the fly's behavioral sensitivity to all light intensities depends on its overall level of light consumption. We tested the effects of this manipulation on both ORN firing rates and behavior, focusing on several different ORN types.

(A) Scaling down all blue light intensities had little effect on the relationship between light intensity and spiking for DM1 ORNs (mean ± s.d.). Data for the standard light levels are reproduced from **Figure S3** (Gal4 line on III).

(B) Scaling down all blue light intensities shifted the intensity-behavior curve to the left for DM1 ORNs (n = 32 and 48 flies, mean ± bootstrapped 95% confidence intervals).

(C) Scaling down all blue light intensities shifted the spiking-behavior curve to the left for DM1 ORNs. Shading indicates bivariate 95% confidence intervals, calculated as in **Figure 4** (see Supplemental Experimental Procedures). Data for the standard light levels are reproduced from **Figure S3B** (Gal4 line on III).

(D-F) Same as (A-C) but for VA2. Again, the spiking-behavior curve is shifted to the left when all blue light intensities are scaled down. Data for the standard light levels are reproduced from **Figure 4**.

(G) Scaling down all blue light intensities shifted the intensity-behavior curve to the left for flies where both DM1 and VA2 expressed channelrhodopsin (mean ± bootstrapped 95% confidence intervals). Data for the low light levels are reproduced from **Figure S5**.

(H) Scaling down all blue light intensities shifted the intensity-behavior curve to the left for VM7 ORNs (mean ± bootstrapped 95% confidence intervals). These experiments used the VM7 Gal4 line on chromosome III. VM7 ORN firing rates were not tested with the lower intensity series.

In summary, we saw that the relationship between light and behavior, and also the relationship between ORNs and behavior, was dependent on the overall level of ORN activity in a given experiment. This implies that higher ORN firing rates produce adaptation in the central circuits that are responsible for these behaviors.
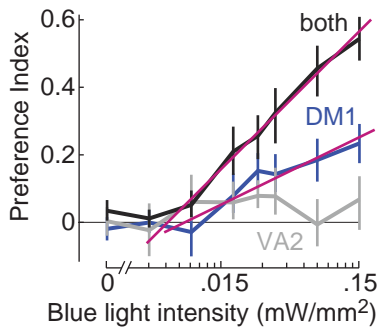
Figure S5: Lack of evidence for lowered behavioral thresholds when attractive glomeruli are co-activated.

Same as **Figure 5A** but for a separate set of experiments where all light intensities were reduced 10-fold, in order to better sample the region of the behavioral threshold. Magenta lines are log-linear fits. Behavioral threshold, as measured by the x-intercept of the fits, is reduced by a small but not statistically significant amount when the two glomeruli are stimulated together, as compared to the situation where DM1 is stimulated alone (p = 0.078; n = 32 for DM1, 40 for VA2, 40 for the combination). Comparison with **Figure 5A** reveals that Preference Index values are overall higher in experiments that use lower light intensities, likely due to de-adaptation of central circuits; see also **Figure S4**.

Figure S6: Twelve behavioral variables measured in individual genotypes.

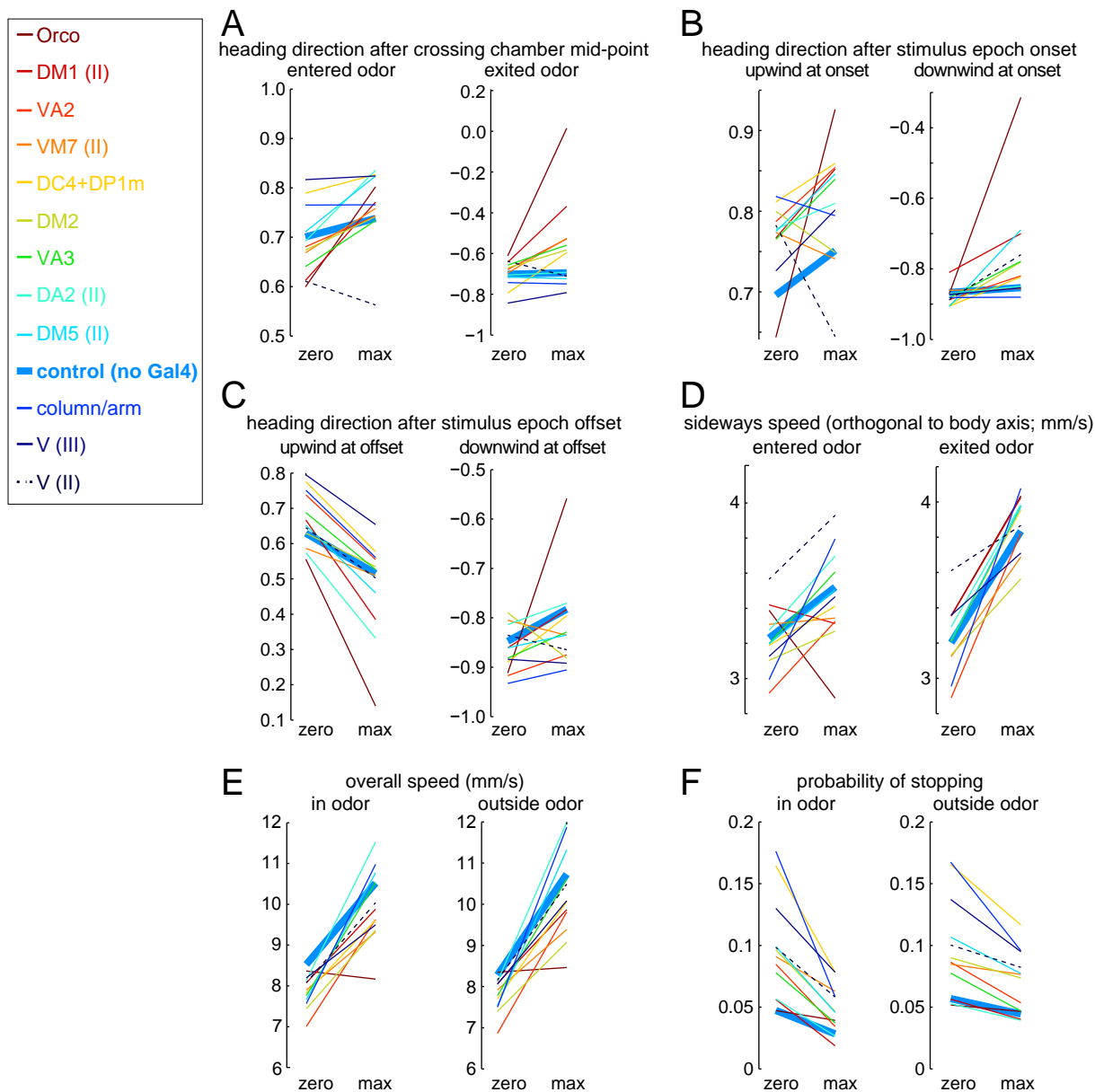Mean values of the 12 behavioral variables analyzed in Figure 8. Color convention is the same as in Figure 8, where warmer colors denote higher Preference Index values. We focus here on the two blue light intensities, zero and maximum.

Note that several variables are relatively consistent across genotypes at zero blue light, and are strongly modulated by light in a genotype-dependent manner. These variables all relate to heading direction after stimulus onset or offset (A, B, C). Note when flies lose the odor at stimulus epoch offset, they tended to reverse heading regardless of whether they were walking upwind or downwind (C); this produced a statistically significant change in their position if they were walking upwind, but if they were walking downwind the resulting change in position was not statistically significant (Figure 3B).

There was one indication of a distinctive behavior in the aversive flies that was independent of the Odor Axis. Namely, the flies that express ChR in V ORNs (using the Gal4 line on chromosome II) tended to reverse after odor zone entry at a rate higher than in zero-blue-laser-trials (panel A). We do not have the statistical power to meaningfully test this result for significance, however. PCA detected this trend, and PC3 was composed mainly of this behavior, but the variance accounted for by this PC did not reach statistical significance.

One caveat in these analyses is that there are variations across genotypes in the basal level (i.e., the zero-blue-light level) of some behaviors. This may be due to long-timescale effects of fictive odor (because zero-blue-light trials are interleaved with other trials). Alternatively, it may be due to differences in genetic background. In framing our conclusions, we have focused on behaviors whose basal level was relatively consistent across genotypes, and which showed reliable genotype-dependent modulation as light intensity increased.
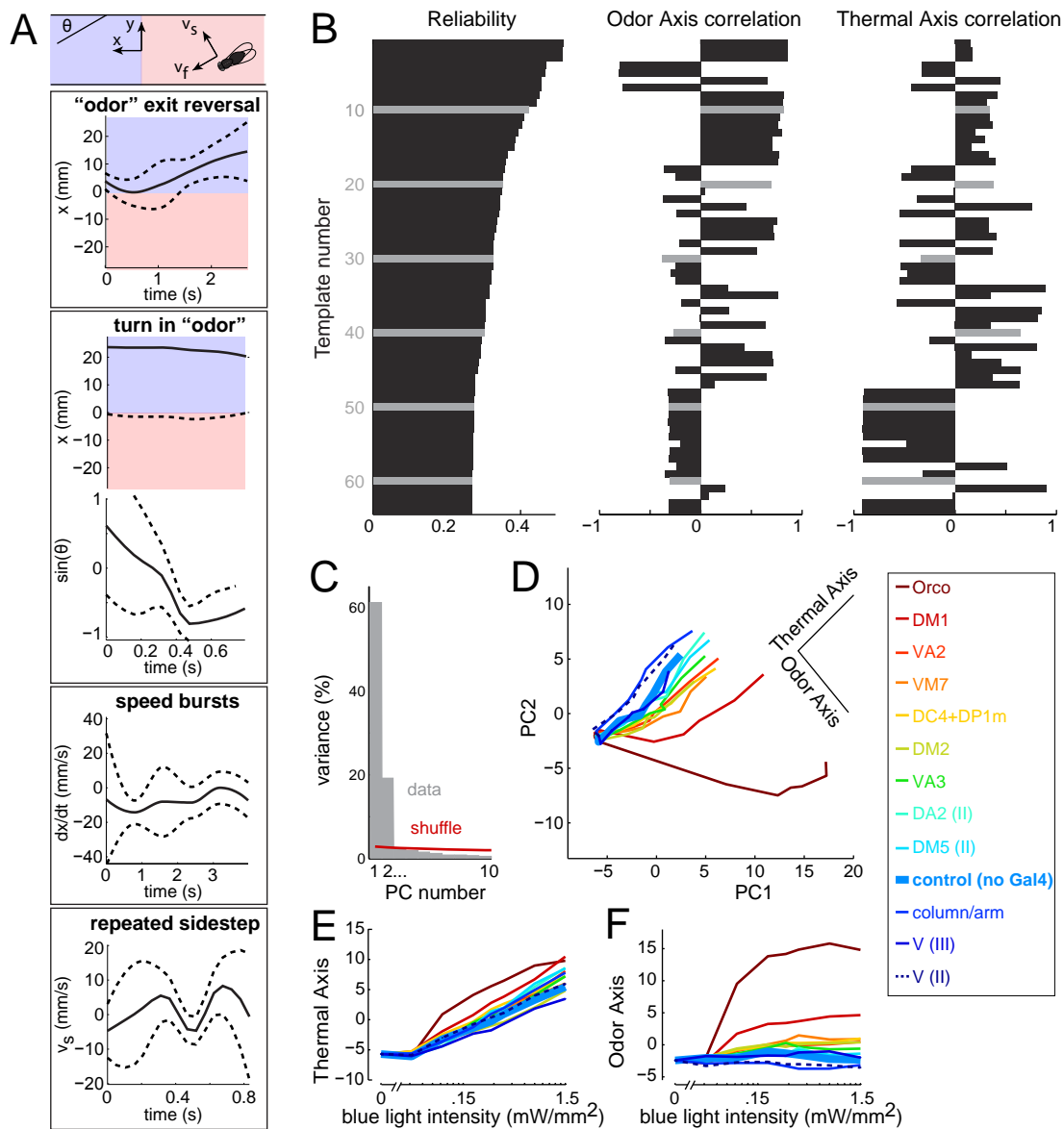
Figure S7. Machine learning approach to behavioral analysis indicates there is only one behavioral program that depends on both blue light intensity and genotype.

(A) Four example behavioral templates. Templates are defined in terms of nine parameters (x, y, dx/dt, dy/dt, sin(θ), cos(θ), dθ/dt, forward velocity, and sideways velocity). Each template is characterized by a constrained range of tolerated values of certain variables, along with complete tolerance for the values of all other variables. Each template is displayed here in the space of the variables that were constrained for that template, with dashed lines indicating the boundaries of the tolerated values and solid lines indicating the mean of those boundary values . Each template was initialized with random tolerances and optimized by gradient descent in order to maximize the reliability of the behavior it detects (see Supplemental Experimental Procedures).

(B) In total we optimized 500 templates. Displayed here are the Reliability scores (see Supplemental Experimental Procedures) for the 64 most reliable templates. Also shown is the correlation with the Odor Axis or the Thermal Axis.

(C) PCA was performed on the scores for all 500 templates, including all the genotypes shown in the inset in panel (D). Plotted here is the fraction of the explainable variance accounted for by the first 10 PCs. The red line shows the upper 95% confidence interval of the result when PCA is performed on shuffled scores. Only the first two PCs are statistically significant.

(D) Behavioral data in the space defined by PC1 and PC2. Each line represents a different genotype, averaged across all flies of that genotype, with different points corresponding to different blue light intensities. Behavior in control flies, which do not express ChR, varies along only one axis in this space (the Thermal Axis). The orthogonal axis (the Odor Axis) accounts for almost all of the explainable variation that depends on genotype.

(E) Projection of the data onto the Thermal Axis, versus blue light intensity. The Thermal Axis is only weakly correlated with PI (R = 0.30).
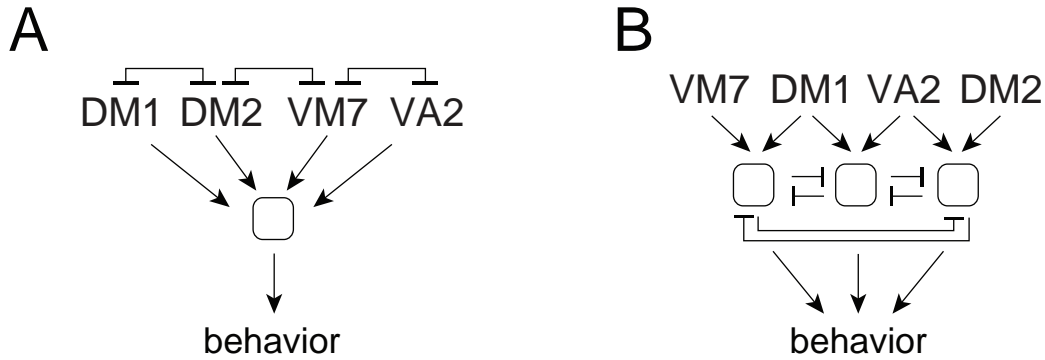
Figure S8. Alternative network implementations of antagonism between olfactory glomeruli.

We found that that behavioral responses to specific pairs of glomeruli summed roughly linearly. However, the effects of other pairs did not sum. In these three latter cases, there was no evidence of summation at even sub-maximal stimulus intensities. In other words, it did not appear that the two components had been summed and then passed through a saturating nonlinearity. Rather, at every stimulus intensity, the contribution of one or both glomeruli appeared to be reduced. This suggests the existence of inhibitory interactions between these pairs of glomeruli. Here we illustrate alternative network implementations of these inhibitory interactions.

(A) A network diagram summarizing the interactions between the four glomeruli in **Figure 5**. Here, individual pairs of glomeruli engage in mutual inhibition, and the surviving outputs of all glomeruli are summed to generate a particular overall level of attraction. These correspond to the three pairs of glomeruli in Figure 5 that showed evidence of a max-pooling operation. Thus, we hypothesize that these mutual inhibitory interactions amount to a winner-take-all competition, or else an incremental reduction in the contribution of each glomerulus so that the result resembles the response to the larger component alone.

(B) An alternative network diagram summarizing the same results. Glomeruli that sum are shown as connecting to the same node. Glomeruli that do not sum are shown as connecting to different nodes. There is mutual inhibition between the nodes, and so co-activating inputs to more than one node reduces the summed behavioral response.

Supplemental Experimental Procedures

Fly care

Flies were raised at 25 ºC on a 12h/12h light-dark cycle on standard cornmeal-molasses medium supplemented with molasses-yeast paste. All flies used for both electrophysiology and behavioral testing were males. Newly eclosed males were collected each day and housed in vials on 10 mL of potato food supplemented with 100 µl of 35 mM all-*trans* retinal (dissolved in ethanol), a chromophore required for ChR activity. Males were placed onto fresh food every 2-3 days. Flies were starved on damp Kimwipes for 12 hours before testing. All flies were 6-8 days old when they were used in either behavioral or electrophysiological experiments. The sequence of trials for each fly lasted approximately 8 hours; flies were tested both during subjective day (beginning at the normal lights-on time) and subjective night (beginning 10 hours after lights-on and ending 6 hours after lights off).

Genotypes

The genotypes used in each figure are listed in **Table S1**. Details regarding the Gal4 lines used to drive transgene expression in specific ORN types are provided in **Table S2**; these lines were originally published in Ai et al. (2010); Couto et al. (2005); Fishilevich and Vosshall (2005); Jones et al. (2007); Silbering et al. (2011); Vosshall et al. (2000); and Wang et al. (2003). We initially selected ORN types for study based on the availability of Gal4 lines. We biased our selection toward neurons with behavioral roles suggested by prior work, and also toward neurons that we were able to record from. A large fraction of OR-Gal4 lines we evaluated did not produce detectable spiking responses to blue light when driving ChR (**Table S2**); we excluded any line that did not produce either a behavioral or electrophysiological response to illumination. To reduce the possibility that behavioral differences between lines could originate from differences in genetic background, we performed experiments whenever possible with two different Gal4 lines targeting the same ORN type (**Figure S3**), and we backcrossed many of our lines (**Table S2**) for at least 10 generations into a common genetic background ("DL", derived from a wild-caught population provided by Michael Dickinson).

To reduce the influence of visual responses to the optogenetic stimuli, we performed all our experiments in $NorpA^7$ hemizygous males (Bloomington Drosophila Stock Center; RRID: BDSC_5685), except as indicated in **Figure S2**. $NorpA^7$ is a *phospholipase C* mutation that eliminates visual transduction (Bloomquist et al., 1988). This mutation eliminated positive phototaxis in control flies (**Figure S2**). We also verified that these flies showed no retinal responses to our stimuli by performing electroretinogram recordings.

To generate experimental flies, males from each Gal4 line were crossed with virgin females bearing the $NorpA^7$ mutation and a UAS-linked transgene encoding a light-activated cation channel (channelrhodopsin-2 containing the H134R mutation and tagged with mCherry; Bloomington Drosophila Stock Center; RRID: BDSC_28995; Pulver et al., 2009). We used confocal imaging of live mCherry fluorescence to verify that ChR expression is restricted to the ORNs projecting to a single glomerulus (data not shown, confirming the results of Couto et al., 2005; Fishilevich and Vosshall, 2005; Silbering et al., 2011). We initially imaged two brains for each of the 15 single-glomerulus genotypes in the study (30 brains total) in order to perform this verification. In three of the 30 brains we observed aberrant widespread expression patterns, but when we re-imaged 14 specimens from each of the two affected genotypes (which harbored the *Or85a-Gal4* line on chromosome II (Fishilevich and Vosshall, 2005), or the *Gr63a-Gal4* line on chromosome III (Jones et al., 2007), we did not encounter these aberrant expression patterns again in any of these 28 brains.

We also confirmed that the *Orco-Gal4* stock we are using drives expression in approximately two-thirds of ORN types (Larsson et al., 2004). It should be noted that Gal4 expression is not uniform across all the *Orco+*

ORN types in this transgenic line (Larsson et al., 2004), and so the behavior we measure may reflect a disproportionate contribution from some of these ORN types.

Finally, we recorded ORN spikes from a subset of the combination genotypes (10 in total) to verify that light evoked spikes in the expected ORN types. In every case we checked, the expected ORNs were indeed responsive to light.

Electrophysiology

We measured neural responses evoked by light using extracellular recordings of ORNs in the antenna and maxillary palp. All data from these experiments are displayed in **Figure S1**. Flies were confined in a pipette tip using dental wax, and the antenna or maxillary palp was immobilized using glass hooks and visualized by an upright microscope (Olympus BX51, 40x air objective). The fly was held in a clean air stream (35 cm/s) and single sensilla were impaled with a sharp glass pipette filled with saline (Schlief and Wilson, 2007). Sensilla were identified by characteristic spike shapes, spontaneous firing rates, and diagnostic odor responses. Responses relative to an eye ground were amplified 100x and low-pass filtered at 5 kHz (AM Systems, Model 2400), and then digitized at 10 kHz (National Instruments, PCI-6251) and stored on a computer for offline analysis. Stimulus lasers were aligned to the fly by imaging the shadow the fly cast in the beam profile.

A few ORN types in our study are not accessible to electrophysiology. However, all these ORN types did elicit behavioral responses. Thus, all the ORN types we studied were validated as light-responsive, using either electrophysiology or behavior (**Table S2**). We discarded genotypes in which light evoked no ORN spikes (**Table S2**).

In **Figure 1**, the ORNs we measure from are all directly illuminated. By contrast, in the behaving fly, some ORNs may be shadowed by the head. This means that the time-averaged ORN firing rates in the behaving fly may be somewhat lower than those in **Figure 1**. Most of the ORN types in this study have overall similar anatomical distributions across the antenna, and therefore their firing rates would be attenuated by the head's shadow in a similar manner. Thus, differential "shadowing" is unlikely to create systematic differences across glomeruli. The only exceptions are the arm/column ORNs, which reside in the sacculus, and VM7 ORNs, which reside in the maxillary palp.

Spike sorting and spike rate analysis

Spike sorting was performed offline using custom software written in MATLAB. We detected spikes by identifying statistically significant peaks in the first derivative of voltage, and then embedded spike waveforms in a two-dimensional space using t-Stochastic Normalized Embedding (t-SNE; van der Maaten and Hinton, 2008). Spikes were then assigned to preliminary clusters using k-means. Superimposed spikes from different neurons in the same sensillum were detected as cluster outliers, and a template matching procedure was used to attempt to fit them as overlapping pairs of spikes. All cluster assignments were verified manually. Peri-stimulus time histograms showing ORN firing rates as a function of time (**Figure S1**) were generated by convolving spike time rasters with a 50-ms Gaussian.

Design and calibration of light stimuli

Light stimuli were generated by blue (445 nm, 500 mW) and red (635 nm, 550 mW) diode lasers (Ultralasers, Inc., Toronto, Canada). Identical lasers were used for electrophysiology and behavioral experiments. In pilot experiments we found that the total spike count from ORNs for a given average light intensity could be maximized by pulsing the beams every 50 ms (20 Hz). Therefore, we used this pulse rate in all our ORN

recordings, and each fly tested behaviorally was also exposed to a pulse of laser illumination every 50 ms during the stimulus epoch. We varied the time-averaged intensity of both lasers by varying the pulse width.

Pilot control experiments showed that *NorpA*[7] flies avoided blue light, likely due to thermal cues (**Figure S2**), so we also illuminated flies with a co-linear red beam pulsed at the same rate. Two-color illumination has been used previously to minimize ChR-independent responses to light in *Drosophila* larvae (Gepner et al., 2015). Adding red light eliminated the tendency of *NorpA*[7] flies to avoid blue light: with the red beam in place, we observed no biases in the choices of *NorpA*[7] flies at the mid-point of the chamber (**Figure S2**). During the stimulus epoch, we adjust the pulse width of both beams to maintain a total optical intensity of 1.5 mW/mm^2, while also varying the fraction of the total intensity carried by the red or blue beam. We used this protocol (where each increment of blue light intensity was traded for an equal increment of red light intensity) because in pilot experiments we found that a red intensity of 1.5 mW/mm^2 happened to be the red intensity that minimized the behavioral bias of *NorpA*[7] flies to blue light of the same intensity (1.5 mW/mm^2) (**Figure S2**). In other words, the point of equiluminance happened to be the point of minimal behavioral bias.

The intensity of both lasers was measured in both the behavior rig and the physiology rig by imaging the beam through a neutral density filter onto a calibrated CCD detector. We needed to perform these measurements because the beam in the behavioral rig was steered by scan mirrors (and also passed through the floor of the acrylic chamber housing the flies), whereas the beam in the physiology rig was not, and so there were some differences in the optical path between the two rigs that could have resulted in different incident power densities at the fly. To achieve the same series of laser intensities at the fly's position in the two rigs, we adjusted the laser pulse durations. Again using measurements with the CCD detector, we verified that the beam size and shape were approximately the same in the two cases. To make additional independent measurements of beam power, we used a calibrated laser power meter (Thorlabs PM-100D), and verified the peak intensity by projecting the center of the beam spot onto a 150 micron diameter pinhole in front of the laser power meter. Measurements with the laser power meter yielded very similar results to our measurements with the calibrated CCD detector .The blue laser intensities we used in our experiments were as follows: 0, 0.045, 0.095, 0.19, 0.28, 0.38, 0.75, and 1.5 mW/mm^2; the only exceptions were **Figures S4** and **S5**, where all these intensities were reduced 10-fold by placing an OD1 neutral density filter in the path of both beams.

Behavior chambers and tracking

In each experiment, eight flies were run simultaneously, each in its own chamber (Claridge-Chang et al., 2009; Parnas et al., 2013). At the beginning of each experiment, each fly was aspirated into a long, narrow plastic chamber measuring 50 x 5 x 1.2 mm. The array of eight chambers was enclosed in a dark box kept at 25 ± 0.5 °C. Charcoal-filtered medical breathing air (35 cm/s) entered each end of each chamber and exited through ports in the center of each chamber. Flies were acclimated to the chambers for 1 hour before testing. Chambers were disassembled and cleaned with water daily. We did not use detergent to avoid contamination, or ethanol because it produced cracking in the acrylic chambers. We used the same chambers throughout the study, so any substances that might have been deposited on the chambers and not removed by the daily cleaning were probably a constant factor throughout the study.

To enable video tracking, the chambers were backlit with infrared light (850 nm). Video data was acquired at 80 Hz using a Unibrain Fire-i Pro camera. A 40 nm wide bandpass infrared filter was mounted in front of the video camera to minimize image contamination by laser light. We tracked the position and orientation of flies in real time using custom software written in MATLAB. We identified flies by background subtraction and thresholding, which produced an ellipse of active pixels. We identified the centroid of the fly via the mean location of thresholded pixels, and the long axis of the fly as the first eigenvector of pixel location covariances. We assumed the head and tail of the fly to be a fixed distances from the centroid along this axis, and we assumed that the head was the end of the ellipse closest to the location of the head on the previous frame. We

distinguished the head of the fly from the tail by assuming that flies never actually made long backwards runs in our behavioral chambers; therefore, if we detected a long backward run (i.e., a run where the time-averaged forward velocity was below a negative-valued threshold), then we assumed this was a tracking error, and we immediately flipped the assumed head location. (Flips were not applied to prior tracking data retroactively.) Flips during laser activation occurred rarely (1.03% of trials).

Real-time video tracking was used to steer a pair of *x-y* scanning galvanometer mirrors (Cambridge Technology, 6215H) that controlled the position of the co-linear blue and red laser beams (**Figure S2**). The lasers were positioned sequentially onto the head of each of 8 simultaneously tracked flies (in separate chambers) so that each fly experienced pulses of light at 20 Hz. The mirrors dwelled at each fly's location for approximately 6 ms before moving to the next fly, regardless of the laser power delivered. Thus, the overall mirror movement frequency was approximately 167 Hz. Mirror retargeting for each jump between adjacent lanes took 0.23 ms. Targeting from the top lane to the bottom lane took 0.5 ms. Laser commands were extinguished a minimum of 0.1 ms before mirror movement to allow laser power output to fall to 0 before the mirrors were moved. The galvanometer mirrors were driven with a custom power supply. Mirror control signals, laser modulation, and camera triggers were output at 200 kHz (National Instruments, PCI-6251).

To assess the tracking accuracy of our system, we measured the median latency between motion in the video field and laser tracking. This latency was approximately 37 ms, with worst case latency less than 46 ms. For a fly briskly walking at 10 mm/s this produces a worst-case tracking error of 460 microns, which is smaller than our beamspot radius of about 750 microns.

Each testing trial consisted of a 60 s pre-stimulus epoch, a 30 s stimulus epoch, and a 60 s post-stimulus epoch. The inter-stimulus interval was 3 min. The intensity of the blue stimulus, and whether it was on the left or right side of the chamber, was varied in a pseudorandom order. We used eight blue light intensities in each experiment, ranging from zero to 1.5 mW/mm^2. When the blue light intensity was less than 1.5 mW/mm^2, we added a compensatory amount of red light to the "odorized" half of the chamber, so that total light intensity was constant at all locations during the stimulus epoch, and across epochs with different blue light intensities. We repeated each blue light intensity 16 times in each experiment, resulting in a total of 5.3 hours of observation for each fly.

As a positive control for our ability to measure a true olfactory behavior in this experimental chamber, we infused one side of the chamber with vinegar odor. This elicited large positive values of the Preference Index, similar to the behavioral response to optogenetic stimulation of *Orco+* ORNs (data not shown). Infusion of concentrated 3-octanol elicited large negative values of the Preference Index (data not shown). The qualitative features of behavior in these experiments were similar to those observed with fictive odors.

In all genotypes, including control flies that lacked Gal4 expression, the stimulus epoch produced a small increase in walking speed that grew with light intensity (**Figure S6**). This behavior is likely triggered by the thermal component of the light stimulus and it does not affect the Preference Index (**Figure 2E**).

Preference Index calculation

We calculated a Preference Index (PI) for each fly to assess attraction to the blue beam following a previously published method (Claridge-Chang et al., 2009; Parnas et al., 2013). We defined a 10 mm "choice zone" at the center of the chamber, identified each time the fly entered this zone, and then counted whether exits from the zone were toward the blue or red side of the chamber. The PI is calculated as

PI = (exits toward blue - exits toward red) / (exits toward blue + exits toward red)

This metric ranges from -1 (maximal repulsion) through 0 (neutrality) to +1 (maximal attraction). An exit from the choice zone toward the blue side was counted as a choice in favor of the fictive odor, whether the fly entered the choice zone from the blue side or the red side. When calculating the PI, exits were pooled across trials with the same stimulus for each fly. Although the Preference Index is computed based only on choices within a small zone at the mid-point of the chamber, it was also highly correlated with the mean fraction of time the fly occupies the blue half of the chamber ($R = 0.95$). We use the term "attraction" to refer to behaviors that increase the PI, simply because these behaviors reflect directed movements in favor of the fictive odor, and these behaviors also increase the proportion of time that the fly spends in the fictive odor.

Statistics

Unless otherwise noted, all error bars denote 95% confidence intervals calculated by bootstrap resampling using the BCa method (Efron and Tibshirani, 1993). Confidence areas for bivariate plots (**Figure 4**) denote the region that contains 95% of linear interpolations between bootstrap samples at each stimulus intensity.

Differences between single-glomerulus genotypes and controls (**Figures 4**, **7B**, and **7F**) were assessed using a bootstrap test (a parametric repeated-measures ANOVA gave similar results). We measured PI at 8 different blue light intensities to produce an intensity-response curve for each genotype, then we calculated the absolute value of the difference between the two curves at each blue light intensity, and finally summed these absolute differences across the 8 intensities. This produces a non-negative test statistic, the integrated absolute difference (IAD), that increases when curves are more different. In short, for each pair of genotypes G1 and G2 we first calculate the test statistic for the data:

$$TS_{data} = IAD(G1, G2)$$

Our null hypothesis is that the two genotypes are actually equivalent. We cannot reject the null hypothesis simply because the IAD>0, because sampling noise would cause the IAD to be nonzero even if the two genotypes being studied were actually identical. Therefore, we used a bootstrap test to assess whether the IAD for each pair of genotypes is greater than expected based on sampling noise. To do this, we simulate the null hypothesis – that the two genotypes were equivalent – by combining all flies from both genotypes into a common pool C. Then, we simulate repetition of the experiment under the null hypothesis by randomly drawing two bootstrap samples of flies B1 and B2 from the common pool C, with replacement. (We choose the sample sizes so that B1 has the same number of flies as G1, and B2 has the same number of flies as G2.) On average, samples B1 and B2 from the common pool C will be identical, but the measured IAD will be greater than 0 because of sampling noise. For each simulated repetition, we calculate the test statistic:

$$TS_{null} = IAD(B1, B2)$$

After many simulated repetitions, the distribution of TS_{null} represents the distribution of the test statistic that we'd expect under the null hypothesis – how large we expect the IAD to be when there is no difference between the genotypes. Finally, we computed the p-value (i.e., the likelihood of the actual test statistic TS_{data} under the null hypothesis) by finding the fraction of experimental replicates that produced an IAD greater than or equal to TS_{data}. This p-value represents the probability of finding a difference from control as large as that produced by the data when there actually was no difference.

Differences between attractive glomeruli alone and combinations of attractive and repulsive glomeruli (**Figure 7**) were assessed using an analogous method.

Linearly summing combinations or max-pooling combinations were simulated by drawing flies with replacement from the combination data after adding an offset to adjust the mean response for each laser

intensity. For the summing models, the mean response was adjusted to equal the sum of the mean component responses. For the max-pooling models, the mean response was adjusted to equal whichever single-glomerulus response was larger for a given light intensity.

Differences between combination intensity series curves and the linear summation models (**Figures 5** and **6**) used the integrated difference between the summation model and the combination response at each laser intensity as the test statistic, under the (one-tailed) null hypothesis that combination responses were not smaller than the summation model.

Differences between the combination intensity series curves and the max-pooling models (**Figure 6**) used the integrated difference between the combination response and the max-pooling model at each laser intensity as the test statistic, under the (one-tailed) null hypothesis that the combination responses were not larger than the max-pooling model. The results of statistical tests in **Figure 6B** are shown using a colormap accessed from ref. (Brewer).

Differences between behavioral thresholds (**Figure S5**) used the x-intercept of a log-linear model fit to the 6 highest laser intensities as the test statistic, under the (one-tailed) null hypothesis that the intercepts of the combinations were not smaller than the intercepts of the components.

Significance of variance described by principal components analysis (**Figure 8, Figure S7**) was assessed by repeatedly shuffling the data matrix to remove covariance between behavioral variables, and plotting the upper 95% confidence interval of the variance explained by each PC of this shuffled matrix.

Several figures (**Figures 4**, **5**, **6**, and **7**) involve multiple statistical tests of a family of related hypotheses, so we corrected for multiple comparisons by applying the Holm-Bonferroni procedure, which limits the family-wise error rate without further assumptions regarding the independence of the hypotheses.

Throughout this study, we use bootstrap procedures to test statistical significance because our primary measure (Preference Index) is bounded on [-1, 1] and is not normally distributed. A bootstrap test was chosen instead of the alternative option (a Kruskal-Wallis non-parametric ANOVA) because the bootstrap is likely to be more powerful, and more sensitive to any non-linear dependence of Preference Index on stimulus intensity. All bootstrap procedures were performed on B=10,000 bootstrap resamples.

Reliability metric

In **Figure 8**, we define a Reliability metric which expresses how consistently a given behavior is modulated by genotype, laser intensity, or both. A maximally reliable behavior would be identical for all flies of the same genotype responding to a particular laser intensity. Consider a vector F containing measurements of a given behavior for all flies over all stimuli (i.e., all genotypes and all laser intensities). The data in this vector is trial-averaged but not fly-averaged, meaning there is one entry in this vector for each tested fly at each laser intensity. We generate a new vector F' by replacing each entry in F with the mean of all entries in F for which the stimulus is the same (i.e., all entries having the same genotype-laser intensity combination). We define the Reliability of this behavior as the variance of F' normalized by the total variance of F:

Reliability = var(F')/var(F)

Reliability is 0 when the average value of F is not different for different stimuli (i.e., if there is no systematic effect of either laser intensity or genotype), and it equals 1 if all the variation in the behavior is entirely predictable based on the identity of the stimulus (the combination of laser intensity and genotype).

Principal components analysis (Signal PCA)

In **Figures 8** and **S7**, to identify the independent axes of stimulus-evoked behavior, as described by our behavioral variables, we performed principal components analysis (PCA). PCA is a linear dimensionality reduction technique that finds a coordinate rotation of the original data to produce an ordered set of uncorrelated scores where the first scores capture as much variance as possible.

We wanted to focus specifically on covariation that is due to the stimulus (the combination of laser intensity and genotype), and not covariation due to unpredictable factors (noise). Therefore, as the input to PCA, we did not use the fly-by-by measurements of each behavioral variable. Rather, we performed PCA on a matrix of responses averaged across all flies receiving each stimulus (i.e., all flies having the same genotype and subjected to the same light intensity), weighted according to the number of flies tested for that stimulus. We term this "Signal PCA".

Specifically, consider a data matrix M, where each row represents the behavioral scores for one fly at one laser intensity, and each column corresponds to a behavioral variable. First, columns of M were z-scored to have 0 mean and unit variance. Next, we generated a matrix of fly-averaged responses M' by, for each column, replacing each entry with the mean of all entries for which the stimulus is the same (i.e., all entries having the same genotype-laser intensity combination).

We then used this matrix M' as the input to the principal components analysis. The result of Signal PCA is a set of scores whose mean stimulus-evoked values are uncorrelated, with the first scores capturing as much of the variance that is explainable by the stimulus as possible. Significance of variance described by each PC was assessed by repeatedly shuffling the data matrix and plotting the upper 95% confidence interval of the variance explained by each PC of this shuffled matrix.

If we included all the genotypes shown in **Figure 8**, then only the first two PCs were statistically significant, and together they accounted for 88% of the variance in the data. Similar results were obtained if *Orco-Gal4* was omitted from the PCA; in this case, PC1 and PC2 accounted for 81% of the variance in the data. Similar results were also obtained if all combination genotypes were included in the PCA; in this case, PC1 and PC2 accounted for 80% of the variance in the data). In all these cases, the control data lies roughly along a straight line in the space defined by PC1 and PC2, and the single-glomerulus genotype with the largest projections onto the Odor Axis is consistently the genotype where ChR2 is expressed in DM1 ORNs.

Template matching gradient-descent

In **Figure 8** we analyzed 12 behavioral variables that seemed likely (based on previous literature) to be components of olfactory navigation in a walking insect (Kennedy, 1977, 1978). In **Figure S7**, we extended this analysis to search for novel behavioral variables using a machine learning algorithm. At each time point, our video tracking algorithm measured the position of the fly's centroid in the *x-y* space of the chamber, as well as the head angle of the fly relative to the long axis of the chamber (θ). Using these measurements, we parameterized walking trajectories as time varying nine-dimensional vectors (**Figure S7**). The nine parameters were: x position, y position, dx/dt, dy/dt, $\sin(\theta)$, $\cos(\theta)$, $d\theta/dt$, velocity along the fly's long axis, and velocity orthogonal to the fly's long axis (**Figure S7A**).

We seeded an initial population of templates by selecting 500 random segments of trace between .5 and 8 s long. Repeated scoring of templates is computationally costly, and this limited the maximum number of templates we could optimize from random segments. However, the fact that we found templates that detected identical kinematic sequences suggests we covered template space densely enough to repeatedly identify the

same templates. For each template we selected 1-4 random dimensions as active for optimization, and required others to remain maximally permissive. Initial tolerances were set to ½,¼,⅛, or $^1/_{16}$ of the maximal range of the dimension.

Behavioral variables were generated from templates by sliding the template along trajectories and counting the fraction of lags for which the trajectory matched the template within the bounds of the tolerances. We calculated the Reliability for the behavioral variable defined by each template, and then used gradient descent to modify each template and associated tolerances to maximize the Reliability. Gradient descent was stopped when no allowed step size improved the Reliability. Following this optimization procedure, more than half of templates produced behavioral variables that were significantly modulated by fictive odors.

Visual inspection showed that the optimized templates were diverse in terms of the parameter values they specified, and the space of tolerances they allowed (**Figure S7A**). Thus, many templates represent distinct reliable behavioral features. Our finding that the behaviors described by these templates are highly correlated with the Preference Index (PI) is therefore not an artifact of gradient descent converging to a common best template. Finally, given these 500 optimized templates, we used PCA (in a manner analogous to **Figure 8**) to identify the independent axes of behavior in this 500-dimensional space (**Figure S7B-F**). Our findings were broadly similar to our findings in **Figure 8** using just 12 behavioral variables suggested by the previous literature. This result makes it less likely that we have missed a critical behavioral variable in our analyses.

References for Supplemental Experimental Procedures

Ai, M., Min, S., Grosjean, Y., Leblanc, C., Bell, R., Benton, R., and Suh, G.S. (2010). Acid sensing by the Drosophila olfactory system. Nature *468*, 691-695.

Bloomquist, B.T., Shortridge, R.D., Schneuwly, S., Perdew, M., Montell, C., Steller, H., Rubin, G., and Pak, W.L. (1988). Isolation of a putative phospholipase C gene of Drosophila, norpA, and its role in phototransduction. Cell *54*, 723-733.

Brewer, C. ColorBrewer: A web tool for selecting colors for maps.

Claridge-Chang, A., Roorda, R.D., Vrontou, E., Sjulson, L., Li, H., Hirsh, J., and Miesenbock, G. (2009). Writing memories with light-addressable reinforcement circuitry. Cell *139*, 405-415.

Couto, A., Alenius, M., and Dickson, B.J. (2005). Molecular, anatomical, and functional organization of the Drosophila olfactory system. Curr. Biol. *15*, 1535-1547.

Efron, B., and Tibshirani, R. (1993). An introduction to the bootstrap (New York: Chapman & Hall).

Fishilevich, E., and Vosshall, L.B. (2005). Genetic and functional subdivision of the Drosophila antennal lobe. Curr. Biol. *15*, 1548-1553.

Gepner, R., Mihovilovic Skanata, M., Bernat, N.M., Kaplow, M., and Gershow, M. (2015). Computations underlying Drosophila photo-taxis, odor-taxis, and multi-sensory integration. Elife *4*, e06229.

Jones, W.D., Cayirlioglu, P., Kadow, I.G., and Vosshall, L.B. (2007). Two chemosensory receptors together mediate carbon dioxide detection in Drosophila. Nature *445*, 86-90.

Kennedy, J.S. (1977). Olfactory responses to distant plants and other odor sources. In Chemical Control of Insect Behavior: Theory and Application, H.H. Shorey, and J.J. McKelvey Jr., eds. (New York: Wiley), pp. 67-91.

Kennedy, J.S. (1978). The concepts of olfactory 'arrestrnent' and 'attraction'. Physiol. Entomol. *3*, 91-98.

Larsson, M.C., Domingos, A.I., Jones, W.D., Chiappe, M.E., Amrein, H., and Vosshall, L.B. (2004). Or83b encodes a broadly expressed odorant receptor essential for Drosophila olfaction. Neuron *43*, 703-714.

Parnas, M., Lin, A.C., Huetteroth, W., and Miesenbock, G. (2013). Odor discrimination in Drosophila: from neural population codes to behavior. Neuron *79*, 932-944.

Pulver, S.R., Pashkovski, S.L., Hornstein, N.J., Garrity, P.A., and Griffith, L.C. (2009). Temporal dynamics of neuronal activation by Channelrhodopsin-2 and TRPA1 determine behavioral output in Drosophila larvae. J. Neurophysiol. *101*, 3075-3088.

Schlief, M.L., and Wilson, R.I. (2007). Olfactory processing and behavior downstream from highly selective receptor neurons. Nat. Neurosci. *10*, 623-630.

Silbering, A.F., Rytz, R., Grosjean, Y., Abuin, L., Ramdya, P., Jefferis, G.S., and Benton, R. (2011). Complementary function and integrated wiring of the evolutionarily distinct Drosophila olfactory subsystems. J. Neurosci. *31*, 13357-13375.

van der Maaten, L., and Hinton, G. (2008). Visualizing data using t-SNE. Journal of Machine Learning Research *9*, 85.

Vosshall, L.B., Wong, A.M., and Axel, R. (2000). An olfactory sensory map in the fly brain. Cell *102*, 147-159.

Wang, J.W., Wong, A.M., Flores, J., Vosshall, L.B., and Axel, R. (2003). Two-photon calcium imaging reveals an odor-evoked map of activity in the fly brain. Cell *112*, 271-282.

Table S1: Genotypes

Note: all flies listed below are males hemizygous for the NorpA[7] mutation. "Y" indicates the male autosome.

Figure Panel	Label	Genotype
Figure 1B		NorpA[7]/Y ; UAS-H134R-ChR2 / + ; Or22a-Gal4 / +
Figure 1C	DM1	NorpA[7]/Y ; UAS-H134R-ChR2 / Or42b-Gal4 ; + / +
	VA2	NorpA[7]/Y ; UAS-H134R-ChR2 / + ; Or92a-Gal4 / +
	VM7	NorpA[7]/Y ; UAS-H134R-ChR2 / Or42a-Gal4 ; + / +
	DM2	NorpA[7]/Y ; UAS-H134R-ChR2 / + ; Or22a-Gal4 / +
	DA2	NorpA[7]/Y ; UAS-H134R-ChR2 / Or56a-Gal4 ; + / +
	DM5	NorpA[7]/Y ; UAS-H134R-ChR2 / Or85a-Gal4 ; + / +
Figure 2B,C,D,F		NorpA[7]/Y ; UAS-H134R-ChR2 / Orco-Gal4 ; + / +
Figure 2E,G	Orco-Gal4	NorpA[7]/Y ; UAS-H134R-ChR2 / Orco-Gal4 ; + / +
	no Gal4	NorpA[7]/Y ; UAS-H134R-ChR2 / + ; + / +
Figure 3		NorpA[7]/Y ; UAS-H134R-ChR2 / Orco-Gal4 ; + / +
Figure 4A	DM1	NorpA[7]/Y ; UAS-H134R-ChR2 / Or42b-Gal4 ; + / +
	VA2	NorpA[7]/Y ; UAS-H134R-ChR2 / + ; Or92a-Gal4 / +
	VM7	NorpA[7]/Y ; UAS-H134R-ChR2 / Or42a-Gal4 ; + / +
	DM2	NorpA[7]/Y ; UAS-H134R-ChR2 / + ; Or22a-Gal4 / +
	DA2	NorpA[7]/Y ; UAS-H134R-ChR2 / Or56a-Gal4 ; + / +
	DM5	NorpA[7]/Y ; UAS-H134R-ChR2 / Or85a-Gal4 ; + / +
Figure 4B	DC4+DP1m	NorpA[7]/Y ; UAS-H134R-ChR2 / Bl ; Ir64a-Gal4 / +
	VA3	NorpA[7]/Y ; UAS-H134R-ChR2 / + ; Or67b-Gal4 / +
Figure 4C	no Gal4	NorpA[7]/Y ; UAS-H134R-ChR2 / + ; + / +
Figure 5A	DM1	NorpA[7]/Y ; UAS-H134R-ChR2 / Or42b-Gal4 ; + / +
	VA2	NorpA[7]/Y ; UAS-H134R-ChR2 / + ; Or92a-Gal4 / +
	both (DM1 + VA2)	NorpA[7]/Y ; UAS-H134R-ChR2 / Or42b-Gal4 ; Or92a-Gal4 / +
Figure 5B	DM2	NorpA[7]/Y ; UAS-H134R-ChR2 / + ; Or22a-Gal4 / +
	VA2	NorpA[7]/Y ; UAS-H134R-ChR2 / + ; Or92a-Gal4 / +
	both (DM2 + VA2)	NorpA[7]/Y ; UAS-H134R-ChR2 / + ; Or22a-Gal4 / Or92a-Gal4
Figure 5C	VM7	NorpA[7]/Y ; UAS-H134R-ChR2 / Or42a-Gal4 ; + / +
	DM1	NorpA[7]/Y ; UAS-H134R-ChR2 / + ; Or42b-Gal4 / +
	both (VM7 + DM1)	NorpA[7]/Y ; UAS-H134R-ChR2 / Or42a-Gal4 ; Or42b-Gal4 / +
Figure 5D	DM1	NorpA[7]/Y ; UAS-H134R-ChR2 / Or42b-Gal4 ; + / +
	DM2	NorpA[7]/Y ; UAS-H134R-ChR2 / + ; Or22a-Gal4 / +
	both (DM1+DM2)	NorpA[7]/Y ; UAS-H134R-ChR2 / Or42b-Gal4 ; Or22a-Gal4 / +
Figure 5E	DM2	NorpA[7]/Y ; UAS-H134R-ChR2 / + ; Or22a-Gal4 / +
	VM7	NorpA[7]/Y ; UAS-H134R-ChR2 / Or42a-Gal4 ; + / +
	both (DM2 + VM7)	NorpA[7]/Y ; UAS-H134R-ChR2 / Or42a-Gal4 ; Or22a-Gal4 / +
Figure 5F	VM7	NorpA[7]/Y ; UAS-H134R-ChR2 / Or42a-Gal4 ; + / +
	VA2	NorpA[7]/Y ; UAS-H134R-ChR2 / + ; Or92a-Gal4 / +
	both (VM7 + VA2)	NorpA[7]/Y ; UAS-H134R-ChR2 / Or42a-Gal4 ; Or92a-Gal4 / +
Figure 6A, row 1	**DM2 + VM7**	**NorpA[7]/Y ; UAS-H134R-ChR2 / Or42a-Gal4 ; Or22a-Gal4 / +**
	DM2	NorpA[7]/Y ; UAS-H134R-ChR2 / + ; Or22a-Gal4 / +

	VM7	NorpA[7]/Y ; UAS-H134R-ChR2 / Or42a-Gal4 ; + / +
	DM2 + DM1	**NorpA[7]/Y ; UAS-H134R-ChR2 / Or42b-Gal4 ; Or22a-Gal4 / +**
	DM2	NorpA[7]/Y ; UAS-H134R-ChR2 / + ; Or22a-Gal4 / +
	DM1	NorpA[7]/Y ; UAS-H134R-ChR2 / Or42b-Gal4 ; + / +
	DM2 + DA2	**NorpA[7]/Y ; UAS-H134R-ChR2 / Or56a-Gal4 ; Or22a-Gal4 / +**
	DM2	NorpA[7]/Y ; UAS-H134R-ChR2 / + ; Or22a-Gal4 / +
	DA2	NorpA[7]/Y ; UAS-H134R-ChR2 / Or56a-Gal4 ; + / +
	DM2 + DC4+DP1m	**NorpA[7]/Y ; UAS-H134R-ChR2 / Bl ; Or22a-Gal4 / Ir64a-Gal4**
	DM2	NorpA[7]/Y ; UAS-H134R-ChR2 / + ; Or22a-Gal4 / +
	DC4+DP1m	NorpA[7]/Y ; UAS-H134R-ChR2 / Bl ; Ir64a-Gal4 / +
	DM2 + VA3	**NorpA[7]/Y ; UAS-H134R-ChR2 / + ; Or22a-Gal4 / Or67b-Gal4**
	DM2	NorpA[7]/Y ; UAS-H134R-ChR2 / + ; Or22a-Gal4 / +
	VA3	NorpA[7]/Y ; UAS-H134R-ChR2 / + ; Or67b-Gal4 / +
	DM2 + DM5	**NorpA[7]/Y ; UAS-H134R-ChR2 / Or85a-Gal4 ; Or22a-Gal4 / +**
	DM2	NorpA[7]/Y ; UAS-H134R-ChR2 / + ; Or22a-Gal4 / +
	DM5	NorpA[7]/Y ; UAS-H134R-ChR2 / Or85a-Gal4 ; + / +
	DM2 + VA2	**NorpA[7]/Y ; UAS-H134R-ChR2 / + ; Or22a-Gal4 / Or92a-Gal4**
	DM2	NorpA[7]/Y ; UAS-H134R-ChR2 / + ; Or22a-Gal4 / +
	VA2	NorpA[7]/Y ; UAS-H134R-ChR2 / + ; Or92a-Gal4 / +
Figure 6A, row 2	**VM7 + DM1**	**NorpA[7]/Y ; UAS-H134R-ChR2 / Or42a-Gal4 ; Or42b-Gal4 / +**
	VM7	NorpA[7]/Y ; UAS-H134R-ChR2 / Or42a-Gal4 ; + / +
	DM1 (III)	NorpA[7]/Y ; UAS-H134R-ChR2 / + ; Or42b-Gal4 / +
	VM7 + DA2	**NorpA[7]/Y ; UAS-H134R-ChR2 / Or42a-Gal4 ; Or56a-Gal4 / +**
	VM7	NorpA[7]/Y ; UAS-H134R-ChR2 / Or42a-Gal4 ; + / +
	DA2 (III)	NorpA[7]/Y ; UAS-H134R-ChR2 / + ; Or56a-Gal4 / +
	VM7 + DC4+DP1m	**NorpA[7]/Y ; UAS-H134R-ChR2 / Or42a-Gal4 ; Ir64a-Gal4 / +**
	VM7	NorpA[7]/Y ; UAS-H134R-ChR2 / Or42a-Gal4 ; + / +
	DC4+DP1m	NorpA[7]/Y ; UAS-H134R-ChR2 / Bl ; Ir64a-Gal4 / +
	VM7 + VA3	**NorpA[7]/Y ; UAS-H134R-ChR2 / Or42a-Gal4 ; Or67b-Gal4 / +**
	VM7	NorpA[7]/Y ; UAS-H134R-ChR2 / Or42a-Gal4 ; + / +
	VA3	NorpA[7]/Y ; UAS-H134R-ChR2 / + ; Or67b-Gal4 / +
	VM7 + DM5	**NorpA[7]/Y ; UAS-H134R-ChR2 / Or42a-Gal4 ; Or85a-Gal4 / +**
	VM7	NorpA[7]/Y ; UAS-H134R-ChR2 / Or42a-Gal4 ; + / +
	DM5 (III)	NorpA[7]/Y ; UAS-H134R-ChR2 / + ; Or85a-Gal4 / +
	VM7 + VA2	**NorpA[7]/Y ; UAS-H134R-ChR2 / Or42a-Gal4 ; Or92a-Gal4 / +**
	VM7	NorpA[7]/Y ; UAS-H134R-ChR2 / Or42a-Gal4 ; + / +
	VA2	NorpA[7]/Y ; UAS-H134R-ChR2 / + ; Or92a-Gal4 / +
Figure 6A, row 3	**DM1 + DA2**	**NorpA[7]/Y ; UAS-H134R-ChR2 / Or42b-Gal4 ; Or56a-Gal4 / +**
	DM1	NorpA[7]/Y ; UAS-H134R-ChR2 / Or42b-Gal4 ; + / +
	DA2 (III)	NorpA[7]/Y ; UAS-H134R-ChR2 / + ; Or56a-Gal4 / +
	DM1 + DC4+DP1m	**NorpA[7]/Y ; UAS-H134R-ChR2 / Or42b-Gal4 ; Ir64a-Gal4 / +**
	DM1	NorpA[7]/Y ; UAS-H134R-ChR2 / Or42b-Gal4 ; + / +
	DC4+DP1m	NorpA[7]/Y ; UAS-H134R-ChR2 / Bl ; Ir64a-Gal4 / +
	DM1 + VA3	**NorpA[7]/Y ; UAS-H134R-ChR2 / Or42b-Gal4 ; Or67b-Gal4 / +**
	DM1	NorpA[7]/Y ; UAS-H134R-ChR2 / Or42b-Gal4 ; + / +
	VA3	NorpA[7]/Y ; UAS-H134R-ChR2 / + ; Or67b-Gal4 / +
	DM1 + DM5	**NorpA[7]/Y ; UAS-H134R-ChR2 / Or42b-Gal4 ; Or85a-Gal4 / +**
	DM1	NorpA[7]/Y ; UAS-H134R-ChR2 / Or42b-Gal4 ; + / +
	DM5 (III)	NorpA[7]/Y ; UAS-H134R-ChR2 / + ; Or85a-Gal4 / +
	DM1 + VA2	**NorpA[7]/Y ; UAS-H134R-ChR2 / Or42b-Gal4 ; Or92a-Gal4 / +**

	DM1	NorpA[7]/Y ; UAS-H134R-ChR2 / Or42b-Gal4 ; + / +
	VA2	NorpA[7]/Y ; UAS-H134R-ChR2 / + ; Or92a-Gal4 / +
Figure 6A, row 4	**DA2 + DC4+DP1m**	**NorpA[7]/Y ; UAS-H134R-ChR2 / Bl ; Or56a-Gal4 / Ir64a-Gal4**
	DA2 (III)	NorpA[7]/Y ; UAS-H134R-ChR2 / + ; Or56a-Gal4 / +
	DC4+DP1m	NorpA[7]/Y ; UAS-H134R-ChR2 / Bl ; Ir64a-Gal4 / +
	DA2 + VA3	**NorpA[7]/Y ; UAS-H134R-ChR2 / + ; Or56a-Gal4 / Or67b-Gal4**
	DA2 (III)	NorpA[7]/Y ; UAS-H134R-ChR2 / + ; Or56a-Gal4 / +
	VA3	NorpA[7]/Y ; UAS-H134R-ChR2 / + ; Or67b-Gal4 / +
	DA2 + DM5	**NorpA[7]/Y ; UAS-H134R-ChR2 / Or85a-Gal4 ; Or56a-Gal4 / +**
	DA2 (III)	NorpA[7]/Y ; UAS-H134R-ChR2 / + ; Or56a-Gal4 / +
	DM5	NorpA[7]/Y ; UAS-H134R-ChR2 / Or85a-Gal4 ; + / +
	DA2 + VA2	**NorpA[7]/Y ; UAS-H134R-ChR2 / Or56a-Gal4 ; Or92a-Gal4 / +**
	DA2	NorpA[7]/Y ; UAS-H134R-ChR2 / Or56a-Gal4 ; + / +
	VA2	NorpA[7]/Y ; UAS-H134R-ChR2 / + ; Or92a-Gal4 / +
Figure 6A, row 5	**DC4+DP1m + VA3**	**NorpA[7]/Y ; UAS-H134R-ChR2 / + ; Ir64a-Gal4 / Or67b-Gal4**
	DC4+DP1m	NorpA[7]/Y ; UAS-H134R-ChR2 / Bl ; Ir64a-Gal4 / +
	VA3	NorpA[7]/Y ; UAS-H134R-ChR2 / + ; Or67b-Gal4 / +
	DC4+DP1m + DM5	**NorpA[7]/Y ; UAS-H134R-ChR2 / Or85a-Gal4 ; Ir64a-Gal4 / +**
	DC4+DP1m	NorpA[7]/Y ; UAS-H134R-ChR2 / Bl ; Ir64a-Gal4 / +
	DM5	NorpA[7]/Y ; UAS-H134R-ChR2 / Or85a-Gal4 ; + / +
	DC4+DP1m + VA2	**NorpA[7]/Y ; UAS-H134R-ChR2 / + ; Ir64a-Gal4 / Or92a-Gal4**
	DC4+DP1m	NorpA[7]/Y ; UAS-H134R-ChR2 / Bl ; Ir64a-Gal4 / +
	VA2	NorpA[7]/Y ; UAS-H134R-ChR2 / + ; Or92a-Gal4 / +
Figure 6A, row 6	**VA3 + DM5**	**NorpA[7]/Y ; UAS-H134R-ChR2 / Or85a-Gal4 ; Or67b-Gal4 / +**
	VA3	NorpA[7]/Y ; UAS-H134R-ChR2 / + ; Or67b-Gal4 / +
	DM5	NorpA[7]/Y ; UAS-H134R-ChR2 / Or85a-Gal4 ; + / +
	VA3 + VA2	**NorpA[7]/Y ; UAS-H134R-ChR2 / + ; Or67b-Gal4 / Or92a-Gal4**
	VA3	NorpA[7]/Y ; UAS-H134R-ChR2 / + ; Or67b-Gal4 / +
	VA2	NorpA[7]/Y ; UAS-H134R-ChR2 / + ; Or92a-Gal4 / +
Figure 6A, row 7	**DM5 + VA2**	**NorpA[7]/Y ; UAS-H134R-ChR2 / Or85a-Gal4 ; Or92a-Gal4 / +**
	DM5	NorpA[7]/Y ; UAS-H134R-ChR2 / Or85a-Gal4 ; + / +
	VA2	NorpA[7]/Y ; UAS-H134R-ChR2 / + ; Or92a-Gal4 / +
Figure 7A	Orco	NorpA[7]/Y ; UAS-H134R-ChR2 / Orco-Gal4 ; + / +
	Orco + V(III)	NorpA[7]/Y ; UAS-H134R-ChR2 / Orco-Gal4 ; Gr63a-Gal4 / +
Figure 7B,C	V(II)	NorpA[7]/Y ; UAS-H134R-ChR2 / Gr63a-Gal4 ; TM2 / +
	V(III)	NorpA[7]/Y ; UAS-H134R-ChR2 / Bl ; Gr63a-Gal4 / +
Figure 7D	**DM1 + V(III)**	**NorpA[7]/Y ; UAS-H134R-ChR2 / + ; Or42b-Gal4 / Gr63a-Gal4**
	DM1	NorpA[7]/Y ; UAS-H134R-ChR2 / + ; Or42b-Gal4 / +
	DM2 + V(III)	**NorpA[7]/Y ; UAS-H134R-ChR2 / Bl ; Or22a-Gal4 / Gr63a-Gal4**
	DM2	NorpA[7]/Y ; UAS-H134R-ChR2 / + ; Or22a-Gal4 / +
	VM7 + V(III)	**NorpA[7]/Y ; UAS-H134R-ChR2 / Or42a-Gal4 ; Gr63a-Gal4 / +**
	VM7	NorpA[7]/Y ; UAS-H134R-ChR2 / Or42a-Gal4 ; + / +
	DM5 + V(III)	**NorpA[7]/Y ; UAS-H134R-ChR2 / Or85a-Gal4 ; Gr63a-Gal4 / +**
	DM5	NorpA[7]/Y ; UAS-H134R-ChR2 / Or85a-Gal4 ; + / +
Figure 7E (left column)	**VA2 + V(II)**	**NorpA[7]/Y ; UAS-H134R-ChR2 / Gr63a-Gal4 ; Or92a-Gal4 / TM2**
	VA2	NorpA[7]/Y ; UAS-H134R-ChR2 / + ; Or92a-Gal4 / +
	DC4+DP1m + V(II)	**NorpA[7]/Y ; UAS-H134R-ChR2 / Gr63a-Gal4 ; Ir64a-Gal4 / TM2**
	DC4+DP1m	NorpA[7]/Y ; UAS-H134R-ChR2 / Bl ; Ir64a-Gal4 / +
	VA3 + V(II)	**NorpA[7]/Y ; UAS-H134R-ChR2 / Gr63a-Gal4 ; Or67b-Gal4 / TM2**

	VA3	NorpA[7]/Y ; UAS-H134R-ChR2 / + ; Or67b-Gal4 / +
	DA2 + V(II)	**NorpA[7]/Y ; UAS-H134R-ChR2 / Gr63a-Gal4 ; Or56a-Gal4 / TM2**
	DA2	NorpA[7]/Y ; UAS-H134R-ChR2 / + ; Or56a-Gal4 / +
Figure 7E (right column)	**VA2 + V(III)**	**NorpA[7]/Y ; UAS-H134R-ChR2 / Bl ; Or92a-Gal4 / Gr63a-Gal4**
	VA2	NorpA[7]/Y ; UAS-H134R-ChR2 / + ; Or92a-Gal4 / +
	DC4+DP1m + V(III)	**NorpA[7]/Y ; UAS-H134R-ChR2 / Bl ; Ir64a-Gal4 / Gr63a-Gal4**
	DC4+DP1m	NorpA[7]/Y ; UAS-H134R-ChR2 / Bl ; Ir64a-Gal4 / +
	VA3 + V(III)	**NorpA[7]/Y ; UAS-H134R-ChR2 / Bl ; Or67b-Gal4 / Gr63a-Gal4**
	VA3	NorpA[7]/Y ; UAS-H134R-ChR2 / + ; Or67b-Gal4 / +
	DA2 + V(III)	**NorpA[7]/Y ; UAS-H134R-ChR2 / Or56a-Gal4 ; Gr63a-Gal4 / +**
	DA2	NorpA[7]/Y ; UAS-H134R-ChR2 / Or56a-Gal4 ; + / +
Figure 7F	column/arm	NorpA[7]/Y ; UAS-H134R-ChR2 / Ir40a-Gal4 ; TM2 / +
Figure 7G	DC4+DP1m	NorpA[7]/Y ; UAS-H134R-ChR2 / Bl ; Ir64a-Gal4 / +
	DC4+DP1m + column/arm	NorpA[7]/Y ; UAS-H134R-ChR2 / Ir40a-Gal4 ; Ir64a-Gal4 / +
Figure 8	Orco	NorpA[7]/Y ; UAS-H134R-ChR2 / Orco-Gal4 ; + / +
	DM1	NorpA[7]/Y ; UAS-H134R-ChR2 / Or42b-Gal4 ; + / +
	VA2	NorpA[7]/Y ; UAS-H134R-ChR2 / + ; Or92a-Gal4 / +
	VM7	NorpA[7]/Y ; UAS-H134R-ChR2 / Or42a-Gal4 ; + / +
	DC4+DP1m	NorpA[7]/Y ; UAS-H134R-ChR2 / Bl ; Ir64a-Gal4 / +
	DM2	NorpA[7]/Y ; UAS-H134R-ChR2 / + ; Or22a-Gal4 / +
	VA3	NorpA[7]/Y ; UAS-H134R-ChR2 / + ; Or67b-Gal4 / +
	DA2	NorpA[7]/Y ; UAS-H134R-ChR2 / Or56a-Gal4 ; + / +
	DM5	NorpA[7]/Y ; UAS-H134R-ChR2 / Or85a-Gal4 ; + / +
	control (no Gal4)	NorpA[7]/Y ; UAS-H134R-ChR2 / + ; + / +
	column/arm	NorpA[7]/Y ; UAS-H134R-ChR2 / Ir40a-Gal4 ; TM2 / +
	V(III)	NorpA[7]/Y ; UAS-H134R-ChR2 / Bl ; Gr63a-Gal4 / +
	V(II)	NorpA[7]/Y ; UAS-H134R-ChR2 / Gr63a-Gal4 ; TM2 / +
Figure S1	DM2	NorpA[7]/Y ; UAS-H134R-ChR2 / + ; Or22a-Gal4 / +
	DM5	NorpA[7]/Y ; UAS-H134R-ChR2 / Or85a-Gal4 ; + / +
	DM1	NorpA[7]/Y ; UAS-H134R-ChR2 / Or42b-Gal4 ; + / +
	DA2	NorpA[7]/Y ; UAS-H134R-ChR2 / Or56a-Gal4 ; + / +
	VM7	NorpA[7]/Y ; UAS-H134R-ChR2 / Or42a-Gal4 ; + / +
	VA2	NorpA[7]/Y ; UAS-H134R-ChR2 / + ; Or92a-Gal4 / +
	V	NorpA[7]/Y ; UAS-H134R-ChR2 / Bl ; Gr63a-Gal4 / +
	VM5d (no ChR) (ab3B ORNs)	NorpA[7]/Y ; UAS-H134R-ChR2 / + ; Or22a-Gal4 / +
Figure S3	DM1 (II)	NorpA[7]/Y ; UAS-H134R-ChR2 / Or42b-Gal4 ; + / +
	DM1 (III)	NorpA[7]/Y ; UAS-H134R-ChR2 / + ; Or42b-Gal4 / +
	VM7 (II)	NorpA[7]/Y ; UAS-H134R-ChR2 / Or42a-Gal4 ; + / +
	VM7 (III)	NorpA[7]/Y ; UAS-H134R-ChR2 / + ; Or42a-Gal4 / +
	DA2 (II)	NorpA[7]/Y ; UAS-H134R-ChR2 / Or56a-Gal4 ; + / +
	DA2 (III)	NorpA[7]/Y ; UAS-H134R-ChR2 / + ; Or56a-Gal4 / +
	DM5 (II)	NorpA[7]/Y ; UAS-H134R-ChR2 / Or85a-Gal4 ; + / +
	DM5 (III)	NorpA[7]/Y ; UAS-H134R-ChR2 / + ; Or85a-Gal4 / +
	V(II)	NorpA[7]/Y ; UAS-H134R-ChR2 / Gr63a-Gal4 ; TM2 / +
	V(III)	NorpA[7]/Y ; UAS-H134R-ChR2 / Bl ; Gr63a-Gal4 / +
Figure S4 A-C	DM1	NorpA[7]/Y ; UAS-H134R-ChR2 / + ; Or42b-Gal4 / +

Figure S4 D-F	VA2	NorpA[7]/Y ; UAS-H134R-ChR2 / + ; Or92a-Gal4 / +
Figure S4G	DM1+VA2	NorpA[7]/Y ; UAS-H134R-ChR2 / + ; Or92a-Gal4 / Or42b-Gal4
Figure S4H	VM7	NorpA[7]/Y ; UAS-H134R-ChR2 / + ; Or42a-Gal4 / +
Figure S5	DM1	NorpA[7]/Y ; UAS-H134R-ChR2 / + ; Or42b-Gal4 / +
	VA2	NorpA[7]/Y ; UAS-H134R-ChR2 / + ; Or92a-Gal4 / +
	both (DM1 + VA2)	NorpA[7]/Y ; UAS-H134R-ChR2 / + ; Or92a-Gal4 / Or42b-Gal4
Figures S6 and S7	Orco	NorpA[7]/Y ; UAS-H134R-ChR2 / Orco-Gal4 ; + / +
	DM1	NorpA[7]/Y ; UAS-H134R-ChR2 / Or42b-Gal4 ; + / +
	VA2	NorpA[7]/Y ; UAS-H134R-ChR2 / + ; Or92a-Gal4 / +
	VM7	NorpA[7]/Y ; UAS-H134R-ChR2 / Or42a-Gal4 ; + / +
	DC4+DP1m	NorpA[7]/Y ; UAS-H134R-ChR2 / Bl ; Ir64a-Gal4 / +
	DM2	NorpA[7]/Y ; UAS-H134R-ChR2 / + ; Or22a-Gal4 / +
	VA3	NorpA[7]/Y ; UAS-H134R-ChR2 / + ; Or67b-Gal4 / +
	DA2	NorpA[7]/Y ; UAS-H134R-ChR2 / Or56a-Gal4 ; + / +
	DM5	NorpA[7]/Y ; UAS-H134R-ChR2 / Or85a-Gal4 ; + / +
	control (no Gal4)	NorpA[7]/Y ; UAS-H134R-ChR2 / + ; + / +
	column/arm	NorpA[7]/Y ; UAS-H134R-ChR2 / Ir40a-Gal4 ; TM2 / +
	V(III)	NorpA[7]/Y ; UAS-H134R-ChR2 / Bl ; Gr63a-Gal4 / +
	V(II)	NorpA[7]/Y ; UAS-H134R-ChR2 / Gr63a-Gal4 ; TM2 / +

Table S2: Gal4 lines

Gal4 line	Glomerulus	Chromo-some	Back-crossed into DL? *	Bloomington Drosophila Stock Center #	Research Resource Identifier (RRID)	Source	Reference
Or22a-Gal4	DM2	3	y	9951	BDSC_9951	L. Vosshall, via Bloomington	Vosshall et al. (2000). Cell 102, 147-159.
Ir40a-Gal4	column/arm	2	n	41727	BDSC_41727	R. Benton, via Bloomington	Silbering et al. (2011). J. Neurosci. 31, 13357-13375.
Or42a-Gal4 (II)	VM7	2	y	*not available*	*not available*	B. Dickson	Couto et al. (2005). Curr. Biol. 15, 1535-1547.
Or42a-Gal4 (III)	VM7	3	n	9969	BDSC_9969	L. Vosshall, via Bloomington	Fishilevich & Vosshall (2005). Curr. Biol. 15, 1548-1553.
Or42b-Gal4 (II)	DM1	2	y	9971	BDSC_9971	L. Vosshall, via Bloomington	Fishilevich & Vosshall (2005). Curr. Biol. 15, 1548-1553.
Or42b-Gal4 (III)	DM1	3	n	9972	BDSC_9972	L. Vosshall, via Bloomington	Fishilevich & Vosshall (2005). Curr. Biol. 15, 1548-1553.
Or56a-Gal4 (II)	DA2	2	n	9988	BDSC_9988	L. Vosshall, via Bloomington	Fishilevich & Vosshall (2005). Curr. Biol. 15, 1548-1553.
Or56a-Gal4 (III)	DA2	3	n	23896	BDSC_23896	B. Dickson, via Bloomington	Couto et al. (2005). Curr. Biol. 15, 1535-1547.
Gr63a-Gal4 (II)	V	2	n	9943	BDSC_9943	L. Vosshall, via Bloomington	Jones et al. (2007). Nature 445, 86-90.
Gr63a-Gal4 (III)	V	3	n	9942	BDSC_9942	L. Vosshall, via Bloomington	Jones et al. (2007). Nature 445, 86-90.
Ir64a-Gal4	DC4+DP1m	3	n	*not available*	*not available*	R. Benton	Ai et al. (2010). Nature 468, 691-695.
Or67b-Gal4	VA3	3	y	*not available*	*not available*	B. Dickson	Couto et al. (2005). Curr. Biol. 15, 1535-1547.
Or85a-Gal4 (II)	DM5	2	n	23133	BDSC_23133	L. Vosshall, via Bloomington	Fishilevich & Vosshall (2005). Curr. Biol. 15, 1548-1553.
Or85a-Gal4 (III)	DM5	3	n	24461	BDSC_24461	L. Vosshall, via Bloomington	Fishilevich & Vosshall (2005). Curr. Biol. 15, 1548-1553.
Or92a-Gal4	VA2	3	y	23139	BDSC_23139	L. Vosshall, via Bloomington	Fishilevich & Vosshall (2005). Curr. Biol. 15, 1548-1553.
Orco-Gal4	many	2	y	26818	BDSC_26818	L. Vosshall, via Bloomington	Wang et al. (2003). Cell 112, 271-282.

* See Supplemental Experimental Procedures: Genotypes.

In single-sensillum recordings, we were unable to detect ORN spiking responses to blue light when driving ChR expression with the following Gal4 lines; therefore, these lines were not used in our experiments.

Or7a-Gal4 (II)	DL5	2	n	23907	BDSC_23907	B. Dickson, via Bloomington	Couto et al. (2005). Curr. Biol. 15, 1535-1547.
Or7a-Gal4 (III)	DL5	3	n	23908	BDSC_23908	B. Dickson, via Bloomington	Couto et al. (2005). Curr. Biol. 15, 1535-1547.
Or10a-Gal4 (II)	DL1	2	y	9944	BDSC_9944	L. Vosshall, via Bloomington	Fishilevich & Vosshall (2005). Curr. Biol. 15, 1548-1553.
Or59b-Gal4 (III)	DM4	3	n	23897	BDSC_23897	B. Dickson, via Bloomington	Couto et al. (2005). Curr. Biol. 15, 1535-1547.
Or82a-Gal4 (III)	VA6	3	y	23126	BDSC_23126	L. Vosshall, via Bloomington	Fishilevich & Vosshall (2005). Curr. Biol. 15, 1548-1553.
Or85b-Gal4 (II)	VM5d	2	n	23911	BDSC_23911	B. Dickson, via Bloomington	Couto et al. (2005). Curr. Biol. 15, 1535-1547.
Or85b-Gal4 (III)	VM5d	3	n	23912	BDSC_23912	B. Dickson, via Bloomington	Couto et al. (2005). Curr. Biol. 15, 1535-1547.

Table S3: Behavioral valence associated with receptors and glomeruli

Receptor	Glomerulus*	Valence	Reference(s)
Or22a	DM2	attraction	Knaden et al. (2012). Cell Rep. 1, 392-399.
		attraction	Semmelhack & Wang (2009). Nature 459, 218-223.
		repulsion	Gao et al. (2015). PLoS One 10, e0125986.
		attraction	*this study*
Or42a	VM7	attraction	Hernandez-Nunez et al. (2015). Elife 4, e06225.
		attraction	Mathew et al. (2013). Proc. Natl. Acad. Sci. USA 110, E2134-2143.
		neutral	Jung et al. (2015) eLife 4:e11092.
		attraction	*this study*
Or42b	DM1	attraction	Semmelhack & Wang (2009). Nature 459, 218-223.
		attraction	Mathew et al. (2013). Proc. Natl. Acad. Sci. USA 110, E2134-2143.
		attraction	Gao et al. (2015). PLoS One 10, e0125986.
		neutral	Jung et al. (2015) eLife 4:e11092.
		attraction	*this study*
Or56a	DA2	repulsion	Stensmyr et al. (2012). Cell 151, 1345-1357.
		attraction	*this study*
Or67b	VA3	attraction	Mathew et al. (2013). Proc. Natl. Acad. Sci. USA 110, E2134-2143.
		attraction	*this study*
Or85a	DM5	attraction	Knaden et al. (2012). Cell Rep. 1, 392-399.
		repulsion	Semmelhack & Wang (2009). Nature 459, 218-223.
		repulsion	Gao et al. (2015). PLoS One 10, e0125986.
		attraction	*this study*
Or92a	VA2	attraction	Semmelhack & Wang (2009). Nature 459, 218-223.
		attraction	Mathew et al. (2013). Proc. Natl. Acad. Sci. USA 110, E2134-2143.
		attraction	Hernandez-Nunez et al. (2015). Elife 4, e06225.
		attraction	*this study*
Ir40a	column/arm	repulsion	Kain et al. (2013).Nature 502, 507-512.
		repulsion	*this study*
Ir64a	DC4/DP1m	repulsion	Ai et al. (2010). Nature 468, 691-695.
		repulsion	Gao et al. (2015). PLoS One 10, e0125986.
		attraction	*this study*
Gr21a/Gr63a	V	repulsion	Suh et al. (2004). Nature 431, 854-859.
		repulsion	Faucher et al. (2006). J. Exp. Biol. 209, 2739-2748.
		repulsion	Suh et al. (2007).Curr. Biol. 17, 905-908.
		repulsion	*this study*

* *Data on larvally-expressed receptors are included here, although the names of larval glomeruli differ from the names of adult glomeruli.*